Inverse Energy-Uncertainty Relation for a Simple Information Engine

Bradley Chase
SFI REU, Summer 2005
Mentor: Alfred Hübler

August 8, 2005

Abstract

We examine the relationship between uncertainty in initial conditions and subsequent energy gain for a simple information engine in the likeness of Maxwell's Demon. Our engine consists of two idealized classical particles in a two-compartment box. Using information about the initial states of the particles and our uncertainty in those states, we desire to capture both particles to perform work. We theorize that in certain cases the energy extracted is inversely proportional to the initial uncertainty and compare this prediction against simulations. We also examine properties of a nonlinear container. We also note that the average energy over all initial condition cases is approximately the fraction of particles which we can predict long enough for the possibility of capture to occur.

1 Introduction and Motivation

The interplay between information and energy first arose from a simple thought experiment devised by James Clerk Maxwell. Imagine a container filled with gas particles, with a removable partition inserted to create two chambers of equal volume. Maxwell's Demon is a tiny being which operates a small trap door on the partition, letting fast particles move to one side of the partition and letting slow particles move to the other side [1]. Without doing any work, the demon has effectively raised the temperature on one side of the partition and lowered it on the other. Such a situation is tantamount to creating order from disorder, a flagrant violation of the second law of thermodynamics. The temperature difference could drive a heat engine, powered continuously by the effortless activities of the demon. A variety of attempts have been made to resolve this paradox, but Leo Szilard was the first to relate the problem to information [2]. In a simplified version of the paradox, which involves a single gas particle and considers pressure rather than temperature, Szilard argued that the act of measurement must bring about an increase in entropy equal to the amount lost when the demon does his work. This measurement and the memory needed to keep it were introduced in terms of bits, an important information measure. However, it was Charles Bennet, influenced by the work of Rolf Landauer, who showed that due to the irreversible nature of the demon's actions, information must be erased, implying a commensurate increase in entropy which accounts

for the later reduction in entropy [3]. This explanation served to firmly relate information and thermodynamics.

While it is clear that the second law of thermodynamics cannot be violated to do work, it is not clear a priori how information itself might be used to do useful work. That is, how can information about a system be used to do work, notwithstanding the increase or at least conservation of entropy that must occur. The applications of such a general information energy conversion are limitless, even for fairly lossy schemes. The possibility of information as a power source is a motivating incentive for considering the relationship of the two quantities. Imagine providing remote power to a laptop simply using information. Since information can be transmitted safely and relatively cheaply, such a scheme would provide an economical source of power. Several considerations have been made regarding the kinetics of such an information engine (see [4]), but little consideration has been given to examining the relationship between information and energy in Szilard's simple system. In this paper, I intend to examine this situation analytically and numerically. In the earlier sections, I derive equations regarding a single particle in a box as well as the propagation of uncertainty. These results are verified against computer simulations. Later sections examine a particular information-energy conversion setup in terms of a Maxwell's Demon type machine.

2 Particle in a Square Box

2.1 Particle Motion

In this simple case, we consider the motion of a particle in a square box with sides of length L. For a particle shot from an initial position x_0, y_0, at an angle θ, we have the position of the particle as a function of time as

$$x = x_0 + t\cos\theta \tag{1}$$
$$y = y_0 + t\sin\theta \tag{2}$$

We wish to calculate the distance the particle travels before it hits the rightmost wall ($x = L$). Using (1), we have

$$\frac{L - x_0}{\cos\theta} = t \tag{3}$$

The distance traveled in each direction is just

$$\Delta x = (L - x_0) \tag{4}$$
$$\Delta y = (L - x_0)\tan\theta \tag{5}$$

Thus the total distance traveled, S, is

$$S = \sqrt{(L - x_0)^2 + (L - x_0)^2\tan\theta^2} \tag{6}$$
$$= (L - x_0)\sqrt{1 - \tan\theta^2} \tag{7}$$
$$= (L - x_0)\csc\theta \tag{8}$$
$$= t \tag{9}$$

The deviation in length, $\frac{\partial S}{\partial x_0}$ is

$$\frac{\partial S}{\partial x_0} = -\frac{1}{\cos\theta}, \quad \frac{\partial S}{\partial y_0} = 0 \tag{10}$$

independent of initial position. Similarly, the deviation in length, $\frac{\partial S}{\partial \theta}$ is

$$\frac{\partial S}{\partial \theta} = \sin\theta \frac{(L - x_0)}{\cos^2\theta} = t\tan\theta \tag{11}$$

which depends on both the initial position and angle.

We are also interested in how the particle will reflect off the wall. Given a surface normal ($\vec{N}$) and direction ($\vec{D}$), the reflected direction ($\vec{R}$) is given by

$$\vec{R} = \vec{D} - (2\vec{D}\cdot\vec{N})\vec{N} \tag{12}$$

For some incident angle (θ_i), we have $\vec{D} = (\cos\theta_i, \sin\theta_i)$. For the right wall, we have $\vec{N} = (-1, 0)$. Then

$$(2\vec{D}\cdot\vec{N}) = -2\cos\theta_i \tag{13}$$

$$\vec{D} - (2\vec{D}\cdot\vec{N})\vec{N} = (-\cos\theta_i, \sin\theta_i) \tag{14}$$

Therefore, $\theta_r = \pi - \theta_i$. The reflected angle is completely independent of the position, and varies with the incident angle as $\frac{\partial \theta_r}{\partial \theta_i} = -1$.

Future bounces will depend on our precision in calculating the collision location. Differentiating (1) and (2), we have

$$\frac{\partial x}{\partial x_0} = 1 + \cos\theta\frac{\partial t}{\partial x_0}, \quad \frac{\partial x}{\partial y_0} = \cos\theta\frac{\partial t}{\partial y_0}, \quad \frac{\partial x}{\partial \theta} = -t\sin\theta + \cos\theta\frac{\partial t}{\partial \theta} \tag{15}$$

$$\frac{\partial y}{\partial x_0} = \sin\theta\frac{\partial t}{\partial x_0}, \quad \frac{\partial y}{\partial y_0} = 1 + \sin\theta\frac{\partial t}{\partial y_0}, \quad \frac{\partial y}{\partial \theta} = t\cos\theta + \sin\theta\frac{\partial t}{\partial \theta} \tag{16}$$

These equations will be used later in determining the propagation of uncertainty in the position and direction of the particle.

2.2 Algorithm for Determining Particle's Path

More generally, given some initial conditions (x_0, y_0, θ_0), we have the ultimate goal of determining when it would hit the partition wall, which depends on the overall path length of the particle. We also want to calculate the uncertainty in this path length.

An algorithm for calculating the trajectory is as follows:

- Given some position and angle, figure out which wall the particle will hit

- Intersect with the wall and calculate the distance traveled

- Using the surface normal of the wall, reflect the particle and restart from the first step

Thus the lifetime of a particle can be considered in terms of sequential wall hits. I will next derive the equations for determining which wall the particle hits and then I will derive the general equations for intersecting and reflecting from the remaining walls.

2.3 Determing Wall Hit

We can imagine drawing vectors connecting the position of the particle to the corners of the box. These vectors will help define the limiting angles which determine the wall hit. The unit vectors to each corner are

$$\vec{v}_{\text{lower left}} = \frac{1}{\sqrt{x_0^2 + y_0^2}}(-x_0, -y_0) \tag{17}$$

$$\vec{v}_{\text{upper left}} = \frac{1}{\sqrt{x_0^2 + (L - y_0)^2}}(-x_0, L - y_0) \tag{18}$$

$$\vec{v}_{\text{upper right}} = \frac{1}{\sqrt{(L - x_0)^2 + (L - y_0)^2}}(L - x_0, L - y_0) \tag{19}$$

$$\vec{v}_{\text{lower right}} = \frac{1}{\sqrt{(L - x_0)^2 + y_0^2}}(L - x_0, -y_0) \tag{20}$$

The unit vector $\vec{z} = (1, 0)$ defines $\theta = 0$. Using the definition of the dot product and the fact that we have unit vectors, we know $\alpha_i = \cos^{-1}(z \cdot v_i)$. So our discriminating angles are

$$\alpha_1 = \cos^{-1}\left(\frac{-x_0}{\sqrt{x_0^2 + y_0^2}}\right) \tag{21}$$

$$\alpha_2 = \cos^{-1}\left(\frac{-x_0}{\sqrt{x_0^2 + (L - y_0)^2}}\right) \tag{22}$$

$$\alpha_3 = \cos^{-1}\left(\frac{L - x_0}{\sqrt{(L - x_0)^2 + (L - y_0)^2}}\right) \tag{23}$$

$$\alpha_4 = \cos^{-1}\left(\frac{L - x_0}{\sqrt{(L - x_0)^2 + y_0^2}}\right) \tag{24}$$

Since $\cos^{-1}\theta$ is multivalued, we need to make sure we have the angle we want. Since, α_1 and α_4 are always pointing to the bottom corners in our system, they should always fall within the range $[\pi, 2\pi]$. Therefore, if either is less than π, we should subtract it from 2π to get the angle we want. Thus, the rules are as follows for determining which wall the particle will hit

- $\alpha_1 > \theta_{\text{particle}}$ and $\theta_{\text{particle}} > \alpha_2$: hits left wall
- $\alpha_2 > \theta_{\text{particle}}$ and $\theta_{\text{particle}} > \alpha_3$: hits top wall
- $\alpha_3 > \theta_{\text{particle}}$ or $\theta_{\text{particle}} > \alpha_4$: hits right wall
- $\alpha_4 > \theta_{\text{particle}}$ and $\theta_{\text{particle}} > \alpha_1$: hits bottom wall

Since we limit the range of theta to $[0, 2\pi]$, we can use the range bounds as implicit limiting angles in the third comparison.
The uncertainty (see [5]) in the calculated angle α_i is given by

$$\delta\alpha_i = \delta x_0 \left|\frac{\partial \alpha_i}{\partial x_0}\right| + \delta y_0 \left|\frac{\partial \alpha_i}{\partial y_0}\right| \tag{25}$$

If $[\theta_{\text{particle}} - \delta\theta_{\text{particle}}, \theta_{\text{particle}} + \delta\theta_{\text{particle}}]$ is not disjoint from all $[\alpha_i - \delta\alpha_i, \alpha_i + \delta\alpha_i]$, then we have lost the ability to predict future motion of the particle.

2.4 Wall intersection and reflections

We now derive the equations for hitting the top, left and bottom walls, noting that we derived the results for hitting the top wall in section 1.

Top Wall

The particle will hit the top wall when $y = L$. In a similar derivation to that in section one, we have the intersection when

$$t = \frac{(L - y_0)}{\sin\theta} \tag{26}$$

and the path distance $S = t$ (the proof is almost identical to that in section one). Therefore, we have our deviations as

$$\frac{\partial S}{\partial x_0} = 0 \tag{27}$$

$$\frac{\partial S}{\partial y_0} = \frac{-1}{\sin\theta} \tag{28}$$

$$\frac{\partial S}{\partial \theta} = -t\cot\theta \tag{29}$$

The unit normal of the top wall is $(0, -1)$. The direction vector is then reflected as $(\cos\theta_i, \sin\theta_i) \rightarrow (\cos\theta_i, -\sin\theta_i)$ or $\theta_r = -\theta_i$. Again, this reflection is independent of position, and $\frac{\partial\theta_r}{\partial\theta_i} = -1$.

Left Wall

A collision with the left wall occurs when $x = 0$, which happens when $t = -x_0/\cos\theta$. Once again, we find that the path length $S = t$. The deviations are then

$$\frac{\partial S}{\partial x_0} = \frac{-1}{\cos\theta} \tag{30}$$

$$\frac{\partial S}{\partial y_0} = 0 \tag{31}$$

$$\frac{\partial S}{\partial \theta} = t\tan\theta \tag{32}$$

The surface normal is $(1, 0)$ which causes a reflection of the direction vector : $(\cos\theta, \sin\theta) \rightarrow (-\cos\theta, \sin\theta)$ or $\theta_r = \pi - \theta_i$. The reflection is again independent of position and varies as $\frac{\partial\theta_r}{\partial\theta_i} = -1$.

Bottom Wall

The particle will hit the top wall when $y = 0$ and

$$t = \frac{(-y_0)}{\sin\theta} \tag{33}$$

Again, the path distance $S = t$. Therefore, we have our deviations as

$$\frac{\partial S}{\partial x_0} = 0 \tag{34}$$

$$\frac{\partial S}{\partial y_0} = \frac{-1}{\sin\theta} \tag{35}$$

$$\frac{\partial S}{\partial \theta} = -t\cot\theta \tag{36}$$

The unit normal of the bottom wall is $(0, 1)$. The direction vector is then reflected as $(\cos\theta_i, \sin\theta_i) \to (\cos\theta_i, -\sin\theta_i)$ or $\theta_r = -\theta_i$. Again, this reflection is independent of position, and $\frac{\partial\theta_r}{\partial\theta_i} = -1$.

The top/bottom pair and the left/right pair have the same deviations. In fact, in comparing the deviations, we see that a re-parametrization of $\theta \to \theta + \pi/2$ and swapping x, y gives the same deviation equations for all four walls.

2.5 Propagation of uncertainty

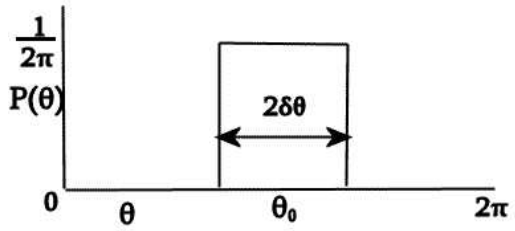

Figure 1: Uncertainty in θ

Assume we have initial conditions and uncertainties $(x_0 \pm \delta x_0, y_0 \pm \delta y_0, \theta_0 \pm \delta\theta_0)$. For example, as depicted in figure 1

$$P(\theta) = \begin{cases} \frac{1}{2\delta\theta_0} \text{ for } \theta_0 - \delta\theta_0 < \theta < \theta_0 + \delta\theta_0 \\ 0 \text{ otherwise} \end{cases} \tag{37}$$

This can be viewed as band-limited white noise, where $2\delta x_0$ would be the bandwidth. Additionally, one could also interpret the quantities as metric or Shannon entropies.

$$H[P(\theta)] = -\int_{-\infty}^{\infty} P(\theta)\ln(P(\theta))d\theta \tag{38}$$

$$= -\int_{\theta_0-\delta\theta_0}^{\theta_0+\delta\theta_0} \frac{1}{2\delta\theta_0}\ln(\frac{1}{2\delta\theta_0})d\theta \tag{39}$$

$$= -\ln(\frac{1}{2\delta\theta_0}) \tag{40}$$

$$= \ln(2\delta\theta_0) \tag{41}$$

For simplicity, we will just consider the uncertainties directly, rather than the

entropic definition. In general, the uncertainties are given by:

$$\delta S = \delta x_0 \left|\frac{\partial S}{\partial x_0}\right| + \delta y_0 \left|\frac{\partial S}{\partial y_0}\right| + \delta\theta_0 \left|\frac{\partial S}{\partial \theta_0}\right| \tag{42}$$

$$\delta x_1 = \delta x_0 \left|\frac{\partial x_1}{\partial x_0}\right| + \delta y_0 \left|\frac{\partial x_1}{\partial y_0}\right| + \delta\theta_0 \left|\frac{\partial x_1}{\partial \theta_0}\right| \tag{43}$$

$$\delta y_1 = \delta x_0 \left|\frac{\partial y_1}{\partial x_0}\right| + \delta y_0 \left|\frac{\partial y_1}{\partial y_0}\right| + \delta\theta_0 \left|\frac{\partial y_1}{\partial \theta_0}\right| \tag{44}$$

$$\delta\theta_1 = \delta\theta_0 \tag{45}$$

Without a major loss of generality, we will consider the case of hitting the right wall. The uncertainty in the parameter t as well as the path length S is

$$\delta t = \delta S = \frac{\delta x_0}{|\cos\theta_0|} + \delta\theta_0 \left|t\tan\theta_0\right| \tag{46}$$

If the particle is moving with speed v, we then know the uncertainty in the time it actually hits the wall is $\delta t/v$. The uncertainty in the next starting position, (x_1, y_1), is determined by equations (15), (16), (43), and (44) using the t parameter from (3). We note here that $\frac{\partial t}{\partial y_0} = 0$.

$$\delta x_1 = \delta x_0 \left|1 + \cos\theta_0 \frac{\partial t}{\partial x_0}\right| + \delta\theta_0 \left|-t\sin\theta_0 + \cos\theta_0 \frac{\partial t}{\partial \theta_0}\right| \tag{47}$$

$$\delta x_1 = \delta x_0 |1-1| + \delta\theta_0 |(-(L-x_0)\tan\theta_0 + (L-x_0)\tan\theta_0| \tag{48}$$

$$\delta x_1 = 0 \tag{49}$$

$$\delta y_1 = \delta x_0 \left|\sin\theta_0 \frac{\partial t}{\partial x_0}\right| + \delta y_0 + \delta\theta_0 \left|t\cos\theta_0 + \sin\theta_0 \frac{\partial t}{\partial \theta_0}\right| \tag{50}$$

$$\delta y_1 = \delta x_0 |\tan\theta_0| + \delta y_0 + \delta\theta_0 \left|\frac{L-x_0}{\cos^2\theta_0}\right| \tag{51}$$

There is no change in the uncertainty in angle, $\delta\theta_1 = \delta\theta_0$
We now consider the particle hitting the bottom wall.

$$\delta t = \delta S = \frac{\delta y_0}{|\sin\theta_0|} + \delta\theta_0 \left|t\cot\theta_0\right| \tag{52}$$

$$\delta x_1 = \delta x_0 + \delta y_0 |\cot\theta_0| + \delta\theta_0 \left|\frac{y_0}{\sin^2\theta_0}\right| \tag{53}$$

$$\delta y_1 = 0 \tag{54}$$

Similar results follow for the remaining two walls. We see then that every time the particle hits a wall, either δx or δy is eliminated.

2.6 Calculating impact time with partition wall and uncertainty

In order to calculate the overall path length and path lifetime (which are proportional), we simply add the individual times t_i for each intermediate wall hit and note the particular time when a wall is hit. We can also calculate the uncertainty in each individual time δt_i. Overall, for k bounces we have

$$T_{\text{total}} \pm \delta T_{\text{total}} = \sum_{i=0}^{k} t_i \pm \sum_{i=0}^{k} \delta t_i \tag{55}$$

where at each step, the uncertainties in x and y increase by equations like those in the previous section. The uncertainty in θ does not change over time.

2.7 Comparison of simulation results and error predictions

In order to check the above equations, a short simulation application was written, the code for which can be seen in listing 1. Given some initial conditions, the code simulates the behavior of the particle in the box. In order to compare deviations in initial positions, the code is run with slightly varying initial conditions. The location, angle, current time and total time are output to a file each time the particle hits a wall.

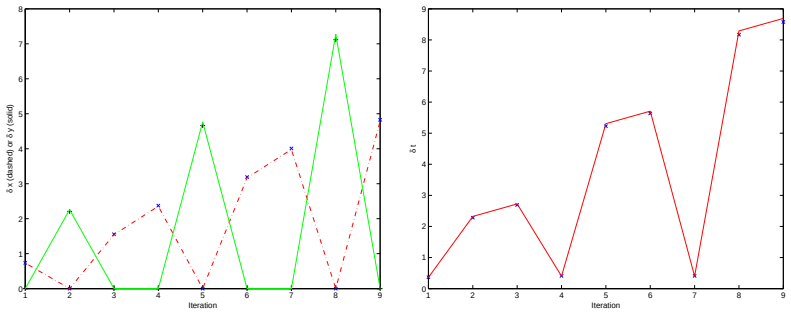

(a) δx and δy (b) δt

Figure 2: Comparison of calculated deviations (dots) and observed deviations (lines) for $\delta x_0 = 0$, $\delta y_0 = 0$ and $\delta\theta_0 = \pi/256$

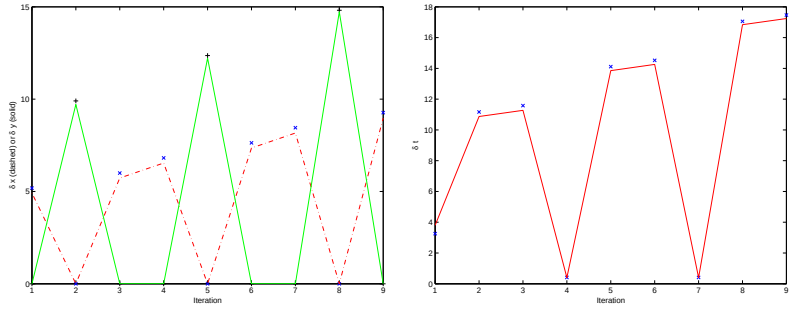

(a) δx and δy (b) δt

Figure 3: Comparison of calculated deviations (dots) and observed deviations (lines) for $\delta x_0 = 2.5$, $\delta y_0 = 3$ and $\delta\theta_0 = \pi/256$

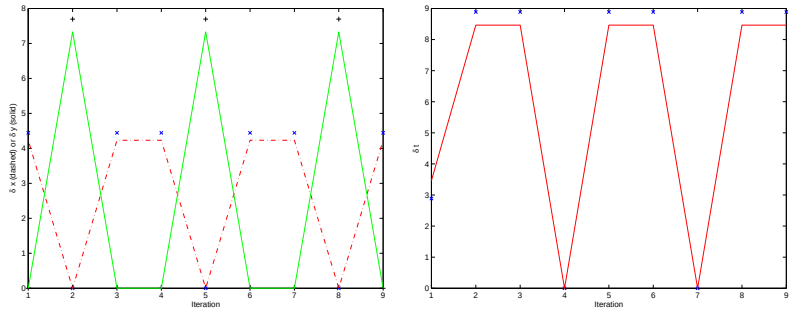

(a) δx and δy (b) δt

Figure 4: Comparison of calculated deviations (dots) and observed deviations (lines) for $\delta x_0 = 2.5$, $\delta y_0 = 3$ and $\delta\theta_0 = 0$

As seen the previous figures, the equations provide an excellent upperbound on the future uncertainty in path length and position. Also, in figures $(4(a), 4(b))$, we see that with no uncertainty in θ_0, there is a global upperbound on δt. More generally, whenever the particle successively hits parallel walls, there is no uncertainty in the path time for that segment.

Listing 1: Simulation Source Code

```
double xpos=(5.0 + 2.5),ypos=5.0,
        theta=M_PI/6.0; /*initial conditions*/
double dt=1e-5;/* timestep */
double L=50; /* wall length */
double t_total=0.0,t_current=0.0;

void simulate(){
  while(1){
    /* collide with walls */
    if(xpos <= 0.0 || xpos >= L){
      theta = M_PI - theta;
      t_current = 0.0;
    }
    if(ypos <= 0.0 || ypos >= L){
      theta *= -1.0;
      t_current = 0.0;
    }
    /* update position */
    xpos = xpos + cos(theta)*dt;
    ypos = ypos + sin(theta)*dt;
    t_total += dt;
    t_current += dt;
  }
}
```

2.8 Ensemble of Particles

To validate the accuracy of the uncertainties in time as listed above, an ensemble of particles was fired and the resulting partition wall hit times were histogrammed. Overlaid on this histogram are bars of width $2\delta t_i$, which represent the uncertainty in hitting at time t_i. The error estimates provide a reasonable

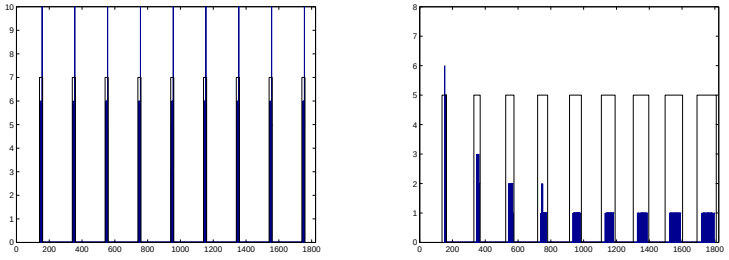

(a) δx and δy (b) δx,δy and δt

Figure 5: Histogram of of particle hit times and calculated hit times and uncertainties

upper bound on the propagated error in both cases.

3 Consideration of Maxwell's Demon

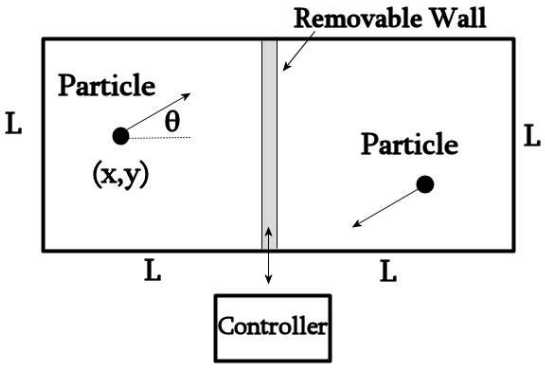

Figure 6: System setup, dashed wall is removable partition

We are now in a position to carefully examine the following experiment. Consider a rectangular box with two equal sized square compartments. Separating these compartments is a partition wall, which can be arbitrarily opened or closed. The box contains two idealized particles, one starting in the left compartment and one starting in the right compartment. An ensemble controller manages the movement of the partition wall. Such a controller simulates a group

of particles uniformly distributed over the initial uncertainty conditions. Using this information, we desire to move the particle in the left compartment to the right compartment. This can be accomplished by opening the partition wall at a time when the left particle would collide with the wall. However, to keep things simple, we guarantee the partition wall is closed when the right particle collides with the wall. In addition to simulating the above engine, we also consider the theory behind the controller behavior. As demonstrated above, uncertainty in the hit time of a particle increases as time goes on. Due to this constraint, we have the following rule–keep the partition wall open unless the right particle might hit it. As a result of this rule, there might be some times when the potential hit times of either particle (the bars in figure 5(a)) overlap. Additionally, the uncertainty for either particle will grow so large that we can no longer predict which wall it will hit. After this time, it is difficult to discuss even probabilistically whether both particles are united. Given the potential hit times, we can calculate the probability that the particle in the left box will make it into the right box.

Let P_0 represent when the particle in the target container hits the wall and P_p represent when the particle in the other container hits the wall.

$$P_p(t) = P_0(t) = \begin{cases} 1 \text{ potential impact} \\ 0 \text{ otherwise} \end{cases} \tag{56}$$

We then have the probability of catching the particle, P_c as

$$P_c = \frac{\int_0^\infty (1 - P_0(t)) P_p(t) dt}{\int_0^\infty P_p(t) dt} \tag{57}$$

Once both particles are on the same side of the partition, we are capable of performing a fixed amount of work from the pressure the particles exert on the partition wall. Adiabatic work done for the two particles is just

$$kT \ln 2 \tag{58}$$

This work or energy is then related to the probability of actually capturing both particles on the same side of the container.

$$W = P_c 2kT \ln 2 \tag{59}$$

3.1 Uncertainty and Energy Relation

As seen in the figure 7, there are 3 nontrivial cases of overlap for which we can calculate the probability that a particle (dashed) is captured. As defined by equation (57), P_c is just the ratio of the non-overlapping area of the red box to the entire area of the dashed box. Here I will derive closed form equations for values of P_c for each of the three cases.

Case 1

$$P_c = \frac{(t_2 + \delta t_2) - (t_1 + \delta t_1)}{2\delta t_2} \tag{60}$$

$$= \frac{(t_2 - t_1) - \delta t_1}{2\delta t_2} + \frac{1}{2} \tag{61}$$

For this overlap to occur, $t_2 - t_1 \leq \delta t_1 + \delta t_2$.

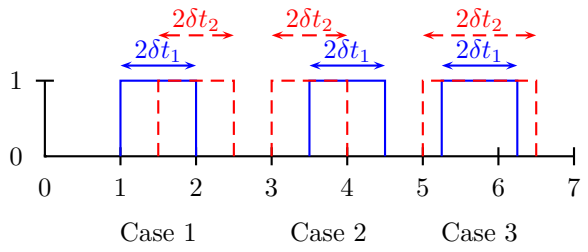

Figure 7: Overlap Cases for Calculating Probability of Capture

Case 2

$$P_c = \frac{(t_1 - \delta t_1) - (t_2 - \delta t_2)}{2\delta t_2} \tag{62}$$

$$= \frac{(t_1 - t_2) - (\delta t_1)}{2\delta t_2} + \frac{1}{2} \tag{63}$$

For this overlap to occur, $t_1 - t_2 \leq \delta t_1 + \delta t_2$.

Case 3

$$P_c = \frac{2\delta t_2 - 2\delta t_1}{2\delta t_2} \tag{64}$$

$$= -\frac{\delta t_1}{\delta t_2} + 1 \tag{65}$$

For this overlap to occur, $\delta t_1 \neq \delta t_2$

The uncertainties in pathlength and equivalently time (for unit velocity) are given by (42). For some set geometry (rectangular box, curve box, etc.), we can look at δt as a function of initial uncertainties in position and angle. We first note that the partial derivatives of S that appear in (42) depend on the geometry and the values of the variables, but are independent of uncertainties. Thus, we need only concern ourselves with the uncertainties in position and angle. In general, the uncertainty in some coordinate q_j on the i-th iteration is

$$\delta q_{j_i} = \sum_k \delta q_{k_{i-1}} \left| \frac{\partial q_j(q_{1_{i-1}}, q_{2_{i-1}}, \ldots)}{\partial q_k} \right| \tag{66}$$

Iterating this equation, we have

$$\delta q_{j_i} = \sum_{k_i} \sum_{k_{i-1}} \cdots \sum_{k_1} \delta q_{k_0} \left| \frac{\partial q_j(q_{1_0}, \ldots)}{\partial q_{k_0}} \right| \cdots \left| \frac{\partial q_j(q_{1_{i-2}}, \ldots)}{\partial q_{k_{i-1}}} \right| \left| \frac{\partial q_j(q_{1_{i-1}}, \ldots)}{\partial q_{k_i}} \right| \tag{67}$$

We see then that the uncertainty δq_{j_i} is entirely linear in terms of initial uncertainties δq_{j_0}. For a given box type and given initial conditions, the uncertainty δt_i is linear in the initial uncertainties. Moreover for these nontrivial cases, the capture probability can be considered as a sum of instances of the

three overlap cases. Looking at each of the three cases as a function of δt, we can in turn relate the overall probability to the initial uncertainty. Since initial conditions are held fixed, t_1 and t_2 are both constant parameters. Case 1 is then just $1/2 + (C_i - \delta t_{1_i})/2\delta t_{2_i}$, case 2 is $1/2 + (C_i - \delta t_{1_i})/2\delta t_{2_i}$ and case 3 is $1 - \delta t_{1_i}/\delta t_{2_i}$, where C_i depends on the geometry of the box and the initial conditions. δt_{1_i} and δt_{2_i} are the uncertainties on the i-th iteration in the hit times of the two particles.

Suppose we have a situation with $a, b,$ and c overlaps of cases 1, 2 and 3 respectively, where $a + b + c = n$. The overall capture probability is then

$$P_c = \frac{1}{n}\left[\sum_{i=1}^{a+b}\left(\frac{1}{2} + \frac{C_i - \delta t_{1_i}}{2\delta t_{2_i}}\right) + \sum_{i=1}^{c}\left(1 - \frac{\delta t_{1_i}}{\delta t_{2_i}}\right)\right] \tag{68}$$

$$= \frac{1}{n}\left[\frac{a}{2} + \frac{b}{2} + c + \sum_{i=1}^{a+b}\frac{C_i - \delta t_{1_i}}{2\delta t_{2_i}} - \sum_{i=1}^{c}\frac{\delta t_{1_i}}{\delta t_{2_i}}\right] \tag{69}$$

$$= \frac{1}{2} + \frac{c}{2n} + \frac{1}{n}\left[\sum_{i=1}^{a+b}\frac{C_i - \delta t_{1_i}}{2\delta t_{2_i}} - \sum_{i=1}^{c}\frac{\delta t_{1_i}}{\delta t_{2_i}}\right] \tag{70}$$

Since C_i is fixed for a given geometry and is independent of δq_{j_0}, the interesting behavior depends on the δt_i's. From (42) and (67), we have

$$\delta t_i = k_1\delta x_0 + k_2\delta y_0 + k_3\delta\theta_0 \tag{71}$$

where the constant coefficients come from summing the partial derivatives in (67).

There are also the two nontrivial cases to consider, in which no overlap occurs resulting in P_c being 0 or 1. The behavior for these cases, which are more common than overlap cases will be discussed later.

3.2 Simulation Verification and Special Cases

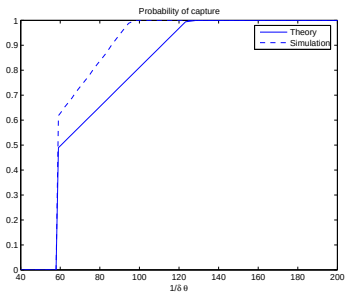

(a) $\theta_{0\text{left}} = 3.3\pi/5, \theta_{0\text{right}} = \pi/3$
Slope = .0079

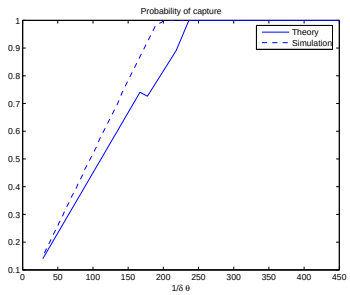

(b) $\theta_{0\text{left}} = 1.01\pi/3, \theta_{0\text{right}} = 2\pi/3$
Slope = .0041

Figure 8: Simulation Verification of $1/\delta t$ behavior

In the simple case when we vary the initial uncertainties together such that $\delta t_2 \approx \delta t_1$, then (70) simplifies to

$$P_c \approx < \frac{C_i}{2\delta t_{2_i}} > \tag{72}$$

Since the energy is proportional to the probability and δt_2 is proportional to the initial uncertainty δ_0, we have

$$E \propto \frac{1}{\delta_0} \tag{73}$$

As seen in figure 8, we observe an inverse relationship between uncertainty and energy for the simple cases in which $\delta\theta_0$ was varied together for both particles. Note that the x-axis in the above plots is in fact $1/\delta\theta_0$, which allows for an easier verification of (72).

While the above analysis focused solely on $\delta\theta_0$, we also examined what happened when we vary δx_0 and δy_0 (figure 9). In subplot (a), we see that if we have a small constant initial δx_0 while varying $\delta\theta_0$, the $\delta t_{1_i} \approx \delta t_{2_i}$ approximation holds and a clear inverse relation is seen. However, as we increase the constant offset, that approximation is no longer true. Instead, the ratio $\delta t_{1_i}/\delta t_{2_i}$ goes as

$$\frac{k_1\delta\theta_0 + \alpha_1}{k_2\delta\theta_0 + \alpha_2} \tag{74}$$

$$= \frac{-k_1}{k_2} + \frac{\alpha_1 - \frac{k_1\alpha_2}{k_2}}{k_2\delta\theta_0 + \alpha_2} \tag{75}$$

For α_2 larger than $k_2\delta\theta_0$, we take a binomial expansion of the denominator in (75), keeping the first two terms

$$\frac{1}{\alpha_2}\left(1 + \frac{k_2\delta\theta_0}{\alpha_2}\right)^{-1} \approx \frac{1}{\alpha_2} - \frac{k_2\delta\theta_0}{\alpha_2^2} \tag{76}$$

Thus, for a larger ambient initial uncertainty, we have a term in P_c which is linear in δq_{j_0} and another term which is inversely related to δq_{j_0} (see 70). Which term dominates depends on the particular conditions involved.

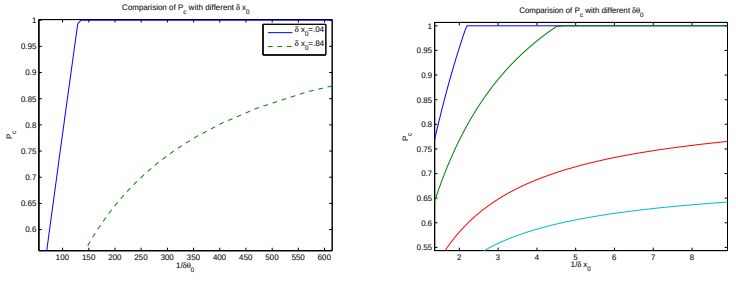

(a) Vary $\delta\theta_0$, Different δx_0 (b) Varying δx_0, with different $\delta\theta_0$

Figure 9: Variation of initial uncertainties

We observe the phenomenon again in subfigure b, where δx_0 and δy_0 were varied for a fixed $\delta\theta_0$. Increased $\delta\theta_0$ are less and less inversely proportional to initial uncertainty, which is seen as less linear in our $1/\delta x_0$ x-axis plot.

We also examined an analogous case in which the upper wall of one container was curved. In this case, the magnitudes of the derivatives in (67) will not necessarily be of the same order, so $\delta t_{1_i} \neq \delta t_{2_i}$. Additionally, the uncertainty in reflected angle is no longer constant, as the curvature increases this uncertainty on every bounce. Consequently, the particle will become unpredictable by this model much sooner than the non-curved case. However, we still expect a result governed by (70), which is essentially inversely proportional to δt_2. Computer simulation verified this expectation, as seen in figure 10, validating our expectation that the geometry should not influence the overlap P_c results. In subplot b, we see that the slope of the $1/\delta\theta_0$ plot decreases linearly as the curvature of the top wall increases. This corresponds to the increased spreading of particle trajectories in the curved case. As we decrease initial uncertainty, we get less of an increase in P_c for this nonlinear case, as the trajectories are more chaotic.

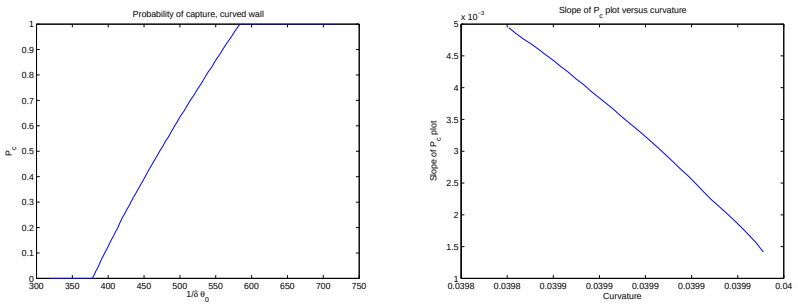

(a) Curved Wall

(b) Curvature-Slope Relation, Slope -31.7275

Figure 10: Simulation Verification for Curved Wall Box

3.3 Averaged Results

The previous section examined special cases which had overlapping hit times . However, there are the other cases where the hit times of particles never overlap, resulting in $P_c = 1$ or 0. This is mostly due to the geometry of the box. For instance, particles shot with the exact same initial conditions will never hit the center wall together. As the particle in the left side approaches the center wall, the particle on the right side would be approaching the rightmost wall. P_c for this case will be 1 unless the initial uncertainty is so large that either particle's behavior becomes unpredictable.

In order to get a sense of the overall energy relationship, we averaged over all possible particle starting positions and angles, varying initial uncertainties. Computationally, this meant we divided each coordinate axis into N initial points, giving N^3 possible initial conditions per particle. For a given uncertainty, we tabulated the hit times and uncertainties according to the derived error

equations. P_c was then calculated pairwise for all initial conditions. These N^6 probabilities were then averaged. The results for a rectangular box are depicted in figure 11. Upwards of ninety-five percent of all initial condition pairs in the

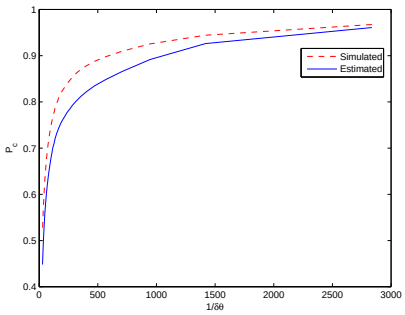

Figure 11: Averaged initial conditions, $N = 50$ steps per coordinate

integration resulted in non-overlapping hit times. The probability of capture P_c is then approximately the ratio of the number of successful captures ($P_c = 1$) to the number of initial condition pairs. Since the number of nonoverlapping and overlapping hit times are determined by both the geometry of the container and the initial uncertainty, an analytic relationship between information and energy is not easily derived. However, we note that the primary source of increasing non-overlap times is the cutoff test described in section 2.3. As we increase the initial uncertainty, we have to cutoff later bounce predictions, as we are unable to predict which wall we hit. However, once a particle reaches $P_c = 0$, it remains so for all higher $\delta\theta_0$, so the curve levels off. Under these assumptions, we have a quasi-linear relationship between $\delta\theta_0$ and the number of $P_c = 0$ particles, with a slope that changes non-continuously according to which bounce iteration is unpredictable. A more precise estimate which also lacks an analytic derivation involves the number of particles which never hit the partition wall. The uncertainty for these particles is so large within the first few bounces that they become unpredictable before they hit the partition wall. The estimate curve above is given by

$$P_{\text{estimate}} = \frac{N^6 - \#\text{ no hits}}{N^6} \tag{77}$$

which implies that the first bounce is the most critical in determining capture.

4 Conclusions and Future Work

We have found a reassuringly intuitive result in examining the relationship between information and energy for particles in a box. Larger initial uncertainty translates into a reduced ability to get energy out of the system. However, we see that geometry and uncertainty play a more complicated role when considering both overlapping and nonoverlapping hit times. Future work includes formalizing this relationship and perhaps devising some analytical equations for other

simple cases. Also, the interplay between δx and δy, particularly the possible distribution of uncertainty between the two over time, could be considered. Another possibility is examining the uncertainty relationship for multiple particles. This will increase the chance of hit overlaps and might tie the integrated behavior more directly to the initial uncertainty. Many physical details could also be considered, including quantum effects, thermal noise, the energy required to run the controller and move the partition wall. We could also examine different controller models rather than the ensemble predictor used here. A search for a maximum efficiency engine would involve comparing different controllers. Attempts to generalize these results to a framework independent of Maxwell's Demon would prove a fruitful step in creating practical information engines.

5 Acknowledgment

Many thanks to Dr. Hubler, whose continual enthusiasm for the project has helped me through many a rough spot. He also provided many great initial ideas for an REU project and I am sorry I only had time to focus on one. Also, thanks to the other REUs for productive tea time discussions and general help. Thanks to the researchers and staff at SFI for providing an amazing environment to work in and for really accepting all of the REU students as active researchers.

A Appendix

A.1 Uncertainty in Wall Classification Angles

The following are the derivatives for the α_i's presented in section (2.3).

$$\frac{\partial \alpha_1}{\partial x_0} = \frac{y_0^2}{(x_0^2+y_0^2)|y_0|} \tag{78}$$

$$\frac{\partial \alpha_1}{\partial y_0} = -\frac{x_0 y_0}{(x_0^2+y_0^2)|y_0|} \tag{79}$$

$$\frac{\partial \alpha_2}{\partial x_0} = \frac{L-y_0}{L^2+x_0^2-2Ly_0+y_0^2} \tag{80}$$

$$\frac{\partial \alpha_2}{\partial y_0} = \frac{x_0}{L^2+x_0^2-2Ly_0+y_0^2} \tag{81}$$

$$\frac{\partial \alpha_3}{\partial x_0} = \frac{L-y_0}{2L^2+x_0^2+y_0^2-2L(x_0+y_0)} \tag{82}$$

$$\frac{\partial \alpha_3}{\partial y_0} = \frac{-L+x_0}{2L^2+x_0^2+y_0^2-2L(x_0+y_0)} \tag{83}$$

$$\frac{\partial \alpha_4}{\partial x_0} = \frac{y_0^2}{(L^2-2Lx_0+x_0^2+y_0^2)|y_0|} \tag{84}$$

$$\frac{\partial \alpha_4}{\partial y_0} = \frac{(L-x_0)y_0}{(L^2-2Lx_0+x_0^2+y_0^2)|y_0|} \tag{85}$$

References

[1] J. C. Maxwell, *Theory of Heat* (Longmans, Green, And Co., London, 1871).

[2] L. Szilard, **53**, (1929).

[3] C. Bennet, Sci. Am. **257**, (1987).

[4] M. M. Millonas, Phys. Rev. Lett. **74**, (1995).

[5] J. R. Taylor, *An Introduction to Error Analysis* (University Science Books, Mill Valley, California, 1982).